14

*Tellus* (1989), *41A*, 179–199

# A study of low-frequency unstable planetary waves in realistic zonal and zonally varying basic states*

By H. L. TANAKA** and ERNEST C. KUNG, *Department of Atmospheric Science, University of Missouri-Columbia, Columbia, MO 65211, USA*

(Manuscript received 12 October 1987; in final form 20 June 1988)

ABSTRACT

This study investigates low-frequency, unstable planetary waves in realistic basis states of January 1979, using three-dimensional spectral primitive equations derived by orthonormal vertical structure functions and Hough harmonics. Eigenfrequencies, modal structures, and energetics are contrasted for the zonal basic state and the zonally varying basic state. Three selected unstable modes are extensively examined. One is the Green mode in the planetary waves, and the other two are deep Charney modes having different meridional structures. We find that the Green mode of wavenumber 1 in the zonally varying basic state shows notable transient growth in the first internal vertical component during its life-cycle. One of the deep Charney modes becomes stationary at a preferred geographical location with nearly barotropic structure. The other deep Charney mode, which shows a monopole structure in the zonal basic state, becomes a dipole structure in the zonally varying basic state. The northern part of the dipole structure shows westward propagation with transient growth in amplitude at a preferred location.

The results suggest that the large-scale Pacific blockings during the winter are, at least in part, related to the low-frequency Charney mode having a dipole structure. A possible connection between the amplification of planetary waves and the Green mode in zonally varying basic states is also discussed.

## 1. Introduction

The problem of large amplification of planetary waves attracts increasingly more attention in association with low-frequency variabilities in the atmosphere. Energetics analyses of the observed circulation field often assert an enhanced baroclinic conversion in the amplified planetary waves, implying that the amplification involves a process of baroclinic instability (e.g., Schilling, 1986). However, the linear stability analyses of planetary waves with zonal basic states (e.g., Simmons and Hoskins, 1976; Hartmann, 1979) indicate major discrepancies with obervations. The expected growth rate is insufficient to explain the amplification, the unstable planetary waves propagate eastward, and the wave structure of the most unstable mode is confined to the troposphere, even though less unstable modes may penetrate into the deep atmosphere.

Comprehensive case studies of blocking episodes during the First GARP (Global Atmospheric Research Program) Global Experiment (FGGE) indicate that synoptic baroclinic waves feed large amounts of energy into the planetary waves by means of an up-scale, nonlinear energy cascade (see Hansen and Chen, 1982; Kung and Baker, 1986; Holopainen and Fortelius, 1987). Long-term statistics of blocking formations also suggest an important role of high-frequency transient eddies in reinforcing the vorticity field of blocking waves (see Colucci, 1985; Mullen, 1987). Although energetics analyses and the enstrophy budget may be helpful in understanding of the causes of blocking formations, the

* Contribution from the Missouri Agricultural Experiment Station Journal Series no. 10440.

** Current affiliation: Geophysical Institute, University of Alaska–Fairbanks, Fairbanks, Alaska, USA.

characteristic structure and behavior of blockings are not fully explained by the energy redistribution due to the wave–wave interaction.

Unstable eigenmodes in a zonally varying basic state were numerically investigted by Simmons et al. (1983), using a barotropic model. They demonstrated that various tropical forcings tend to excite a unique, unstable normal mode in the model atmosphere. Moreover, with his two-layer, quasi-geostrophic model, Frederiksen (1982) showed that the zonal asymmetry of the basic state reorganizes the synoptic baroclinic waves to yield the Atlantic and Pacific storm tracks. Presumably his high-frequency synoptic disturbances are associated with Charney type instability in a zonal basic state. He also found blocking-like unstable modes with a dipole structure among a number of unstable solutions. He proposed that the dipole unstable mode explains the onset of the blocking formation. However, the physical explanation of the dipole modes seems less clear than the high-frequency synoptic disturbances. Although Frederiksen and Bell (1987) have extended his model to a five-layer tropospheric model, the structure and behavior of their eigenmodes in planetary waves are too complicated to relate to the well-known unstable modes of Charney and Green types in a zonal basic state. It is desirable for the modal identification to compare both the unstable modes in a zonal basic state and those in a zonally varying basic state. It is also desirable to use primitive equations because the quasi-geostrophic equations involve quasi-nondivergent and quasi-geostrophic assumptions, which may affect eigensolutions for planetary waves.

The objective of this study was to investigate the low-frequency, unstable planetary waves in realistic global basic states of January 1979 during the FGGE. The eigenfrequencies, modal structures, and energetics of low-frequency unstable solutions are contrasted for zonal and zonally varying basic states in order to examine the effect of zonal asymmetry of the basic state on the low-frequency, unstable planetary waves. For that purpose, we have solved linearized, three-dimensional spectral primitive equations with a basis of three-dimensional normal mode functions (3-D NMFs) of motionless atmosphere. The use of the normal mode expansion is advantageous for stability analysis because the matrix size for the eigenevalue problem can be efficiently reduced by retaining only the rotational mode basis, and excluding the gravity mode basis. Thus, it is possible to analyze atmospheric eigenmodes with primitive equations, not only for zonal basic states but also for zonally varying basic states. Although our eigenvalue problem may be solved for any realistic basic state, complicating the basic state might cause the modal identification and physical interpretation of the eigensolutions to be lost. In this study we have considered a zonally varying basic state which is specified by a steady wavenumber 2, superimposed on the zonal mean basic state.

First the governing equations in terms of the three-dimensional, spectral primitive equations are reduced to the eigenvalue problem. The results for the zonal basic states are presented to identify the unstable modes with Charney (1947) and Green (1960) modes in previous research. We then examine how the zonal asymmetry of the basic state modulates the unstable planetary waves. Finally we discuss the relation between the results of low-frequency unstable modes and the observed large-scale Pacific blockings and the amplification of wavenumber 1 during the winter season.

## 2. Governing equations

### *2.1. Primitive equations with a static stability parameter*

A system of primitive equations in a spherical coordinate of longitude $\lambda$, latitude $\theta$, pressure $p$, and time $t$ may be reduced to three prognostic equations of horizontal motions and thermodynamics with three dependent variables ($u$, $v$, and $\phi$). Here, $u$ and $v$ are the zonal and meridional components of the horizontal velocity $V$. The variable $\phi$ is a departure of the local isobaric geopotential from the reference state geopotential $\phi_0$, which is related through the hydrostatic equation to the reference state temperature $T_0$. Using a matrix notation, these primitive equations (refer to Holton, 1975; Tanaka, 1985) may be written as:

$$M\frac{\partial}{\partial t}W + LW = N + F, \tag{1}$$

where

$$W = (u, v, \phi)^{\mathrm{T}}, \tag{2}$$

$$M = \mathrm{diag}\left(1, 1, -\frac{\partial}{\partial p}\frac{p^2}{R\gamma}\frac{\partial}{\partial p}\right), \tag{3}$$

$$L = \begin{bmatrix} 0 & -2\Omega\sin\theta & \dfrac{1}{a\cos\theta}\dfrac{\partial}{\partial\lambda} \\ 2\Omega\sin\theta & 0 & \dfrac{1}{a}\dfrac{\partial}{\partial\theta} \\ \dfrac{1}{a\cos\theta}\dfrac{\partial}{\partial\lambda} & \dfrac{1}{a\cos\theta}\dfrac{\partial(\ )\cos\theta}{\partial\theta} & 0 \end{bmatrix}, \tag{4}$$

$$N = \begin{bmatrix} -\boldsymbol{V}\cdot\nabla u - \omega\dfrac{\partial u}{\partial p} + \dfrac{\tan\theta}{a}uv \\ -\boldsymbol{V}\cdot\nabla v - \omega\dfrac{\partial v}{\partial p} - \dfrac{\tan\theta}{a}uu \\ \dfrac{\partial}{\partial p}\left(\dfrac{p^2}{R\gamma}\boldsymbol{V}\cdot\nabla\dfrac{\partial\phi}{\partial p} + \omega p\dfrac{\partial}{\partial p}\left(\dfrac{p}{R\gamma}\dfrac{\partial\phi}{\partial p}\right)\right) \end{bmatrix}, \tag{5}$$

$$\boldsymbol{F} = \left(F_u, F_v, \frac{\partial}{\partial p}\left(\frac{pQ}{c_p\gamma}\right)\right)^{\mathrm{T}}. \tag{6}$$

The left-hand side of (1) represents linear matrix operators $M$ and $L$ and a dependent variable vector $\boldsymbol{W}$. The right-hand side represents a nonlinear term vector $\boldsymbol{N}$ and a diabatic term vector $\boldsymbol{F}$, which includes the zonal $F_u$ and meridional $F_v$ components of frictional forces and a diabatic heating rate $Q$. The superscript T denotes transpose, the symbol $a$ represents the earth's radius, $\Omega$ the angular speed of the earth's rotation, $R$ the specific gas constant, $c_p$ the specific heat at a constant pressure, and $\nabla$ the horizontal del-operator. Refer to Table 1 for symbols, definitions, and variables used in this study. The vertical $p$-velocity $\omega$ is related to mass divergence, and the static stability parameter $\gamma$ is given by

$$\gamma = \frac{RT_0}{c_p} - p\frac{\mathrm{d}T_0}{\mathrm{d}p}, \tag{7}$$

in which $T_0$ is assumed to be a function of $p$ alone. In (5), as seen in Holton (1975), a vertical advection term of perturbation temperature is retained discarding the vertical change of $\gamma$ in order to satisfy an energy conservation requirement.

Table 1. *Symbols, definitions, and variables*

| | |
|---|---|
| $\lambda$ | longitude |
| $\theta$ | latitude |
| $p$ | pressure |
| $t$ | time |
| $s$ | zonal wavenumber |
| $l$ | meridional index |
| $m$ | vertical index |
| $S$ | truncation of $s$ |
| $L$ | truncation of $l$ |
| $M$ | truncation of $m$ |
| $T_0$ | reference state temperature |
| $\phi_0$ | reference state isobaric geopotential |
| $u$ | zonal wind speed |
| $v$ | meridional wind speed |
| $\phi$ | isobaric geopotential deviation from $\phi_0$ |
| $\boldsymbol{V}$ | horizontal wind velocity |
| $z$ | height (vertical velocity = dz/dt) |
| $\omega$ | vertical $p$-velocity (= d$p$/d$t$) |
| $\gamma$ | static stability parameter |
| $a$ | radius of the earth |
| $g$ | earth's gravity |
| $\Omega$ | angular speed of earth's rotation |
| $R$ | specific gas constant of dry air |
| $c_p$ | specific heat at constant pressure |
| $F_u$ | zonal component of frictional force |
| $F_v$ | meridional component of frictional force |
| $Q$ | diabatic heating rate |
| $p_s$ | surface pressure of reference state |
| $\tilde{t}$ | dimensionless time scaled by $2\Omega$ |
| $\nabla$ | horizontal del-operator |
| $\delta_{ij}$ | kronecker delta |
| $i$ | imaginary unit |
| $M$ | linear matrix operator given by (3) |
| $L$ | linear matrix operator given by (4) |
| $\boldsymbol{W}$ | dependent variable vector $(u, v, \phi)^{\mathrm{T}}$ |
| $\boldsymbol{N}$ | nonlinear term vector given by (5) |
| $\boldsymbol{F}$ | diabatic term vector given by (6) |
| $h_m$ | equivalent height |
| $c_m$ | phase speed of gravity waves associated with $h_m$ |
| $X_m$ | scaling matrix for $\boldsymbol{W}$ |
| $Y_m$ | scaling matrix for $\boldsymbol{F}$ |
| $\langle\ ,\ \rangle$ | inner product defined by (12) |
| diag( ) | diagonal matrix |
| $(\ )^{\mathrm{T}}$ | transpose of a vector |
| $(\ )^*$ | complex conjugate |
| $(\ )_{\mathrm{R}}$ | real part |
| $(\ )_{\mathrm{I}}$ | imaginary part |
| $(\bar{\ })$ | time-independent basic state |
| $(\ )_{slm}$ | a component of indices $s$, $l$, $m$ |
| $(\ )_i$ | abbreviation of $(\ )_{slm}$ used for perturbations |
| $(\ )_j$ | abbreviation of $(\ )_{s'l'm'}$ used for perturbations |
| $(\ )_k$ | abbreviation of $(\ )_{s'l'm'}$ used for basic states |
| $(\ )_s$ | a component of a wavenumber $s$ |
| $(\ )_{m=0}$ | barotropic component |

Table 1—*continued*

| | |
|---|---|
| $(\ )_{m\neq 0}$ | baroclinic component |
| $\Pi_{slm}$ | 3-D NMF in a resting atmosphere |
| $\sigma_{slm}$ | dimensionless eigenfrequency of Laplace's tidal equation |
| $w_{slm}$ | expansion coefficient of $W$ |
| $f_{slm}$ | expansion coefficient of $F$ |
| $r_{ijk}$ | real interaction coefficient for indices $i, j, k$ |
| $K$ | dimension of a system (14) |
| $N$ | matrix size of a system (16) |
| $w$ | dependent variable vector $(w_1, \ldots, w_N)^T$ |
| $f$ | external forcing vector $(f_1, \ldots, f_N)^T$ |
| $B$ | complex matrix associated with $w$ |
| $C$ | complex matrix associated with $w^*$ |
| $D$ | real diagonal matrix composed of $\sigma_i$ |
| $b_{ij}$ | $(i, j)$ entry of $B$ given by (20) |
| $c_{ij}$ | $(i, j)$ entry of $C$ given by (21) |
| $\nu$ | eigenfrequency of systems (24) and (26) |
| $\xi, \zeta$ | eigenvectors of systems (24) and (26) |
| $E_i$ | perturbation energy of a component $i$ (i.e., $s, l, m$) |
| $C(B, E)$ | energy transformation from a basic state to perturbations |
| $M_1$ | deep Charney mode (stationary mode) |
| $M_2$ | deep Charney mode (dipole mode) |
| $M_C$ | shallow Charney mode |
| $M_G$ | internal Green mode |

### 2.2. *Spectral primitive equations*

In order to obtain spectral primitive equations, we assume that the vectors $\boldsymbol{W}$ and $\boldsymbol{F}$ in (1) can be approximated by a finite series of three-dimensional, normal mode functions in a resting atmosphere $\Pi_{slm}(\lambda, \theta, p)$:

$$\boldsymbol{W}(\lambda, \theta, p, t) = \sum_{s=-S}^{S} \sum_{l=0}^{L} \sum_{m=0}^{M} w_{slm}(t)\, X_m \boldsymbol{\Pi}_{slm}(\lambda, \theta, p), \tag{8}$$

$$\boldsymbol{F}(\lambda, \theta, p, t) = \sum_{s=-S}^{S} \sum_{l=0}^{L} \sum_{m=0}^{M} f_{slm}(t)\, Y_m \boldsymbol{\Pi}_{slm}(\lambda, \theta, p). \tag{9}$$

Here the expansion coefficients $w_{slm}$ and $f_{slm}$ are the functions of time alone. The subscripts represent zonal wavenumbers $s$, meridional indices $l$, and vertical indices $m$. They are truncated at $S$, $L$, and $M$, respectively. The scaling matrices should be defined for each vertical index as:

$$X_m = \mathrm{diag}(c_m, c_m, c_m^2), \tag{10}$$

$$Y_m = \mathrm{diag}(2\Omega c_m, 2\Omega c_m, 2\Omega), \tag{11}$$

where $c_m$ is a phase speed of gravity waves in shallow water, associated with the equivalent height $h_m$. The expansion basis $\Pi_{slm}(\lambda, \theta, p)$ is given by a tensor product of vertical structure functions (vertical normal modes) and Hough harmonics (horizontal normal modes). It is known that they form a complete set and satisfy an orthonormality condition under an inner product $\langle\ ,\ \rangle$ as:

$$\begin{aligned}\langle \boldsymbol{\Pi}_{slm}, \boldsymbol{\Pi}_{s'l'm'} \rangle &= \frac{1}{2\pi p_s} \int_0^{p_s} \int_{-\pi/2}^{\pi/2} \int_0^{2\pi} \boldsymbol{\Pi}^*_{slm} \cdot \boldsymbol{\Pi}_{s'l'm'} \cos\theta \, d\lambda \, d\theta \, dp \\ &= \delta_{ss'} \delta_{ll'} \delta_{mm'},\end{aligned} \tag{12}$$

where the asterisk denotes the complex conjugate, the symbol $\delta_{ij}$ is the Kronecker delta, and the surface pressure $p_s$ is treated as a constant near the earth's surface.

Applied to the inner product for (1), the weak form of primitive equation becomes

$$\left\langle M \frac{\partial}{\partial t} \boldsymbol{W} + L\boldsymbol{W} - \boldsymbol{N} - \boldsymbol{F},\ Y_m^{-1} \boldsymbol{\Pi}_{slm} \right\rangle = 0. \tag{13}$$

Substituting (8) and (9) into (13), rearranging the time-dependent variables, and evaluating the remaining terms, we obtain a three-dimensional, spectral primitive equation as a system of ordinary differential equations with external forcing terms,

$$\frac{dw_i}{d\tilde{t}} + i\sigma_i w_i = -i \sum_{j=1}^{K} \sum_{k=1}^{K} r_{ijk} w_j w_k + f_i, \qquad i = 1, 2, \ldots, K, \tag{14}$$

where $\tilde{t} = 2\Omega t$, $K = (2S+1)(L+1)(M+1)$, $i$ the imaginary unit, and $\sigma_i$ the dimensionless eigenfrequencies obtained as a solution of Laplace's tidal equation with a basic state at rest. For simplicity, the three triple subscripts $slm$, $s'l'm'$, and $s''l''m''$ have been shortened to subscripts $i$, $j$, and $k$, respectively. There should be no confusion in the use of $i$ for a subscript even though it is used for the imaginary unit. The real interaction coefficients $r_{ijk}$ are explicitly evaluated by the triple product of the basis functions. Analytical expression is available for derivatives of $\Pi_{slm}(\lambda, \theta, p)$. We should note here that the zonal wavenumbers $s$, $s'$, and $s''$ run from the negative integer $-S$ to the positive integer $S$, including zero, by definition of the Fourier series.

According to the Galerkin procedure above, the system satisfies the same boundary conditions as 3-D NMFs in a resting atmosphere. Thus

for the boundary conditions it may be reasonable to assume a vanishing kinematical wind, $(u, v, \mathrm{d}z/\mathrm{d}t) = 0$, near the lower surface and a bounded energy at the upper limit of the atmosphere (see Staniforth et al., 1985). The application of such a 3-D NMF expansion is widely seen in the nonlinear normal mode initialization technique which provides successful initial data for prediction models.

### 2.3. Perturbation method

Next, if we introduce a perturbation method using notations $\bar{w}_i$ and $\bar{f}_i$ for time-independent basic states and $w_i$ and $f_i$ for small perturbations superimposed on the basic states (the same symbols with the original variables are used for convenience), the equation for the first-order term of perturbations becomes

$$\frac{\mathrm{d}w_i}{\mathrm{d}\tilde{t}} + i\sigma_i w_i = -i \sum_{j=1}^{K} \left( \sum_{k=1}^{K} (r_{ijk} + r_{ikj}) \bar{w}_k \right) w_j + f_i, \quad i = 1, 2, \ldots, K, \tag{15}$$

where the modal index $k$ is used for the basic state and $i$ and $j$ for the perturbations. Since the negative zonal wavenumbers represent complex conjugates of the positive zonal wavenumbers, we can rewrite the equation above in terms of a matrix form for $s \geqslant 0$:

$$\frac{\mathrm{d}}{\mathrm{d}\tilde{t}} w + iDw = -iBw - iCw^* + f, \tag{16}$$

where

$$w = (w_1 \ldots w_i \ldots w_N)^{\mathrm{T}}, \quad \text{for } s \geqslant 0, \tag{17}$$

$$f = (f_1 \ldots f_i \ldots f_N)^{\mathrm{T}} \quad \text{for } s \geqslant 0, \tag{18}$$

$$D = \mathrm{diag}(\sigma_1 \ldots \sigma_i \ldots \sigma_N), \tag{19}$$

and $N = (S+1)(L+1)(M+1)$. The $(i, j)$ entries of the complex matrices $B$ and $C$, $b_{ij}$ and $c_{ij}$, are determined by the expansion coefficients of the basic state:

$$b_{ij} = \sum_{k=1}^{K} (r_{ijk} + r_{ikj}) \bar{w}_k, \quad i, j = 1, 2, \ldots, N \quad \text{for } s' \geqslant 0, \tag{20}$$

$$c_{ij} = \sum_{k=1}^{K} (r_{ijk} + r_{ikj}) \bar{w}_k, \quad i, j = 1, 2, \ldots, N \quad \text{for } s' < 0. \tag{21}$$

In this study, an inviscid and adiabatic eddy will be examined, disregarding $f$ for perturbations. Both $B$ and $C$ vanish for a basic state at rest ($\bar{w}_k = 0$), thus the equation (16) satisfies Laplace's classical tidal theory.

### 2.4. Eigenvalue problems

For a zonal basic state ($\bar{w}_k \neq 0$ if $s'' = 0$), the matrix $B$ becomes a real block diagonal ($b_{ij} \neq 0$ if $s = s'$), and $C$ vanishes. Consequently (16) can be solved for each $(s, s')$ block:

$$\frac{\mathrm{d}}{\mathrm{d}\tilde{t}} w_s = -iD_s w_s - iB_s w_s, \quad s = 1, 2, \ldots, S, \tag{22}$$

where the subscripts represent wavenumbers of $(s, s')$ blocks associated with perturbation vectors $w_s$. Because (22) is linear, we can assume the solution of $w_s$ to be

$$w_s(\tilde{t}) = \xi \exp(-i\nu\tilde{t}). \tag{23}$$

The initial value problem (22) is then reduced to an eigenvalue problem for a real matrix with eigenvectors $\xi$ and eigenvalues $\nu$ as:

$$\nu\xi = (D_s + B_s)\xi. \tag{24}$$

For a zonally varying basic state, both matrices $B$ and $C$ in (16) become complex, full matrices. Because of the complex conjugate term, we cannot simply assume an exponential-type solution as in (23). In this case the complex matrices and variables are split into real and imaginary parts (subscripts R and I, respectively), and a solution is sought in the form:

$$\begin{bmatrix} w_{\mathrm{R}} \\ w_{\mathrm{I}} \end{bmatrix} (\tilde{t}) = \begin{bmatrix} \xi \\ \zeta \end{bmatrix} \exp(\nu\tilde{t}). \tag{25}$$

The eigenvalue problem for (16) then becomes:

$$\nu \begin{bmatrix} \xi \\ \zeta \end{bmatrix} = \begin{bmatrix} B_{\mathrm{I}} + C_{\mathrm{I}} & B_{\mathrm{R}} - C_{\mathrm{R}} + D \\ -B_{\mathrm{R}} - C_{\mathrm{R}} - D & B_{\mathrm{I}} - C_{\mathrm{I}} \end{bmatrix} \begin{bmatrix} \xi \\ \zeta \end{bmatrix}. \tag{26}$$

For complex eigenpairs the real-valued eigensolutions are given by

$$\begin{bmatrix} w_{\mathrm{R}} \\ w_{\mathrm{I}} \end{bmatrix} (\tilde{t}) = 2 \exp(\nu_{\mathrm{R}}\tilde{t}) \left( \begin{bmatrix} \xi_{\mathrm{R}} \\ \zeta_{\mathrm{R}} \end{bmatrix} \cos \nu_{\mathrm{I}}\tilde{t} - \begin{bmatrix} \xi_{\mathrm{I}} \\ \zeta_{\mathrm{I}} \end{bmatrix} \sin \nu_{\mathrm{I}}\tilde{t} \right). \tag{27}$$

Eqs. (24) and (26) are thus to be solved for zonal and zonally varying basic states in the subsequent sections.

### 2.5. Truncations

In this study, twelve vertical structure functions ($m = 0$–11) are constructed numerically after Kasahara (1984) with 24 Gaussian levels. The vertical index $m = 0$ is called an external (barotropic) mode, and $m = 1$–11 are called internal (baroclinic) modes which have $m$ nodes in the vertical. The numerical internal modes are the discrete approximation of the continuous spectrum. Table 2 lists the reference state temperature $T_0$ on 24 Gaussian levels and the obtained equivalent heights $h_m$ for $m = 0$–11. The global mean temperature for the FGGE year (see Tanaka, 1985) is interpolated onto the Gaussian levels up to 30 mb, and the temperature of the standard atmosphere is substituted above this level. the temperature profile for the FGGE year is very close to that for every monthly mean. The

Table 2. *The reference state temperature $T_0$ at the 24 Gaussian levels and the equivalent heights $h_m$ for the vertical modes $m = 0$–11*

| Level | $T_0$ (K) | Level | $T_0$ (K) | $m$ | $h_m$ (m) |
|---|---|---|---|---|---|
| 1 | 253.78 | 13 | 262.63 | 0 | 9746.5 |
| 2 | 226.08 | 14 | 267.89 | 1 | 3457.7 |
| 3 | 215.39 | 15 | 272.26 | 2 | 777.5 |
| 4 | 211.41 | 16 | 275.92 | 3 | 269.3 |
| 5 | 206.01 | 17 | 279.03 | 4 | 113.9 |
| 6 | 208.23 | 18 | 281.71 | 5 | 46.9 |
| 7 | 216.04 | 19 | 284.04 | 6 | 24.1 |
| 8 | 223.23 | 20 | 286.03 | 7 | 13.5 |
| 9 | 231.44 | 21 | 287.66 | 8 | 7.7 |
| 10 | 240.42 | 22 | 288.94 | 9 | 3.7 |
| 11 | 248.86 | 23 | 289.83 | 10 | 1.2 |
| 12 | 256.31 | 24 | 290.33 | 11 | 0.1 |

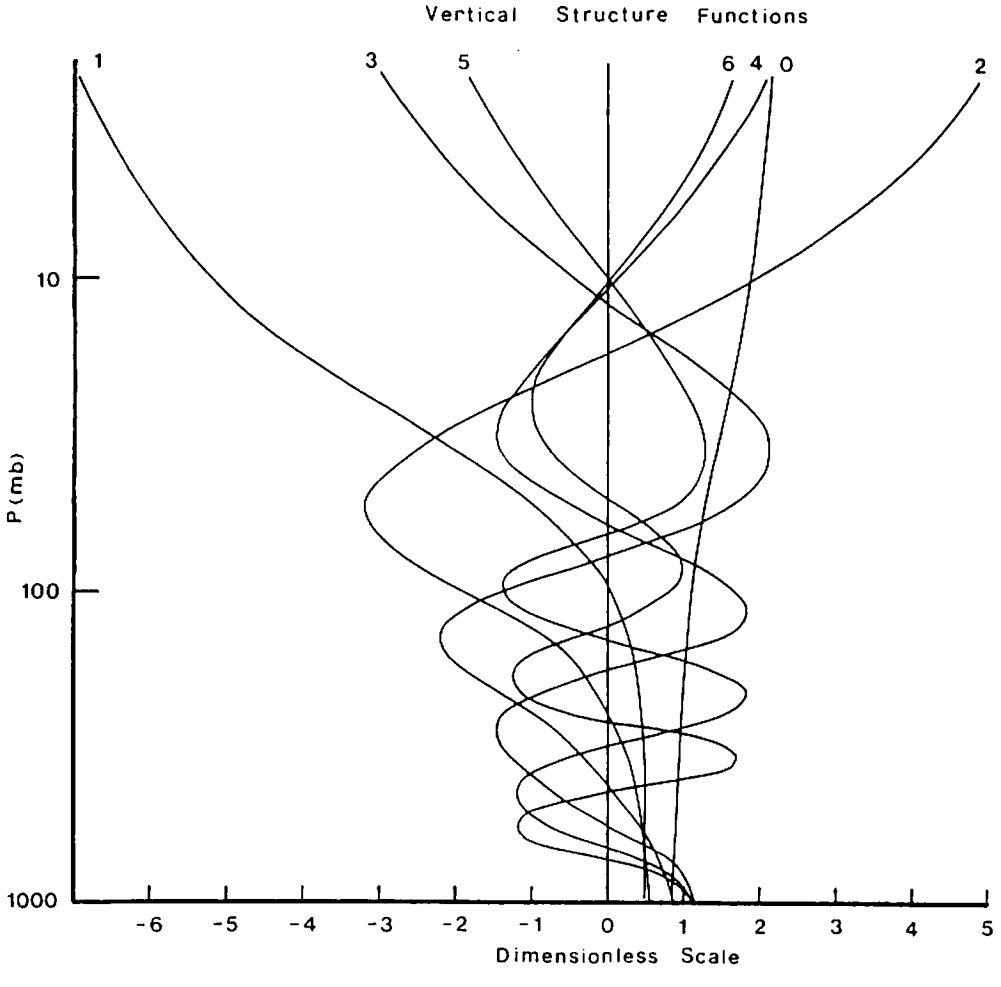


*Fig. 1.* Vertical structure functions for vertical indices $m = 0$–6. Values of corresponding equivalent heights are seen in Table 2.

difference is at most 2 K at the lower troposphere. Since the higher order internal modes have a problem of aliasing in the stratosphere and above (refer to Sasaki and Chang, 1985; Staniforth et al., 1985), only the first seven vertical structure functions ($m = 0$–6) are applied to the subsequent computations (i.e., $M = 6$). Fig. 1 illustrates these vertical structure functions. They may be suitable for the representation of planetary waves because they provide adequate vertical resolutions throughout the troposphere and the stratosphere. As is demonstrated by the resolution test in the Appendix, the unstable modes in the planetary waves have almost converged by this vertical resolution.

The Hough vector functions are computed using semi-normalized associated Legendre polynomials with 120 Gaussian latitudes so that the integral is exact up to the triple product of the basis functions. The meridional indices $l$ contain two distinct modes: gravity–inertia modes and rotational modes of the Rossby–Haurwitz type. One advantage of Hough mode expansion is an efficient reduction of the matrix size of the instability problems by retaining the rotational mode basis alone, excluding the gravity mode basis. As is shown in the Appendix, excluding the gravity mode basis does not affect the unstable solutions of planetary waves. Moreover, the unstable solutions have almost converged with meridional truncation $L = 18$ using the rotational modes. We choose $L = 18$ in this study. In addition we include the Kelvin mode using a numbering of $l = -1$ because the observed energy level is exceptionally large among the gravity modes. According to the observed energy spectra by Tanaka (1985), these vertical and meridional truncations represent about 90% of the total energy of the atmosphere.

## 3. Results for zonal basic states

### 3.1. Basic states

Unstable eigenmodes are examined for two different zonal basic states: a zonal wind profile of a 30° jet described by Simmons and Hoskins (1976) and the observed monthly-mean field of January 1979. The 30° jet profile has a separable structure in the vertical and the meridional, and is deliberately chosen to be barotropically stable (refer to Simmons and Hoskins, 1976). The January basic state is compiled with the FGGE III-b data assimilated by the Geophysical Fluid Dynamics Laboratory. Fig. 2 illustrates the latitude-height section of the observed monthly-mean zonal wind field reproduced by $m'' = 0$–6 and $l'' = 0$–18 of the geostrophic modes.

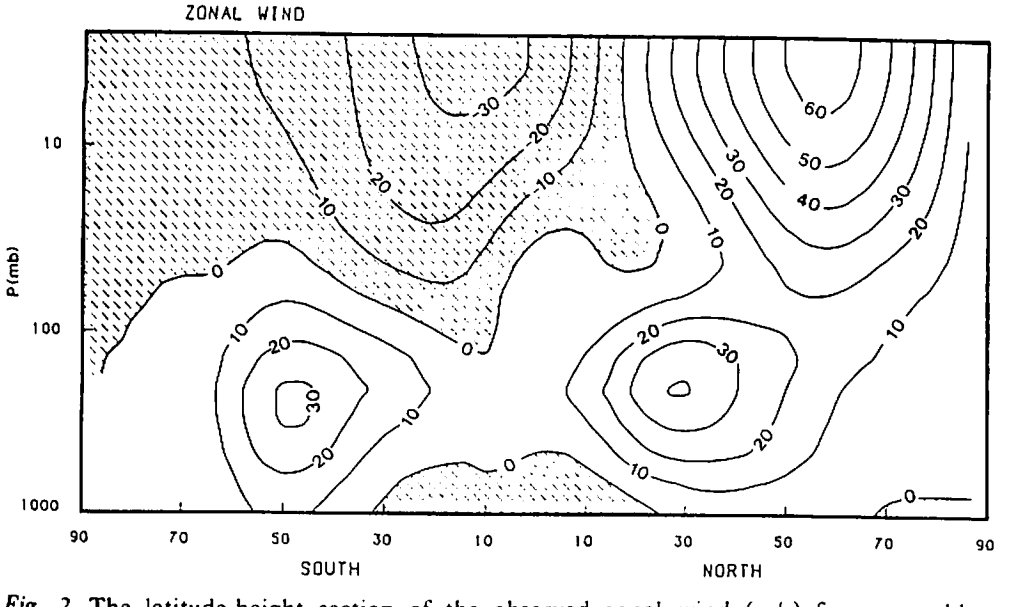


*Fig. 2.* The latitude-height section of the observed zonal wind (m/s) for a monthly-mean of January 1979, reproduced by $l'' = 0$–18 and $m'' = 0$–6.

*3.2. Growth rates and phase speeds*

The growth rates and phase speeds of the first-three unstable modes are plotted in Fig. 3 as functions of the zonal wavenumbers $s = 1$–$10$. This is a result of antisymmetric solutions with the 30° jet basic state. Since the stratosphere is not considered in Simmons and Hoskins' 30° jet, we first compute the fastest growing modes using a constant $\gamma = 30$ K (cross mark), and compare them with Simmons and Hoskins' results (white circle). The value of the constant $\gamma$ represents its vertical average (see Table 1 of Tanaka, 1985). The agreement is within a reasonable range. Henceforth the results are based on the temperature profile in Table 2. A pronounced Charney-type baroclinic instability (labeled $M_C$) appears with the e-folding time of about 2.0 (day) at $s = 7$–$8$ with the phase speed of about 9 (°/day). Contrasted with the result by Simmons and Hoskins (1976), we find that the stable layer in the stratosphere reduces the growth rates for $s > 6$, and the maximum growth rates shift toward smaller wavenumbers. According to Ioannou and Lindzen's (1986) analytical solutions, the unstable modes in the figure, $M_C$, $M_2$, and $M_1$, can be identified as Charney modes with different meridional structures. The phase speed of $M_1$ is very slow in the planetary waves,

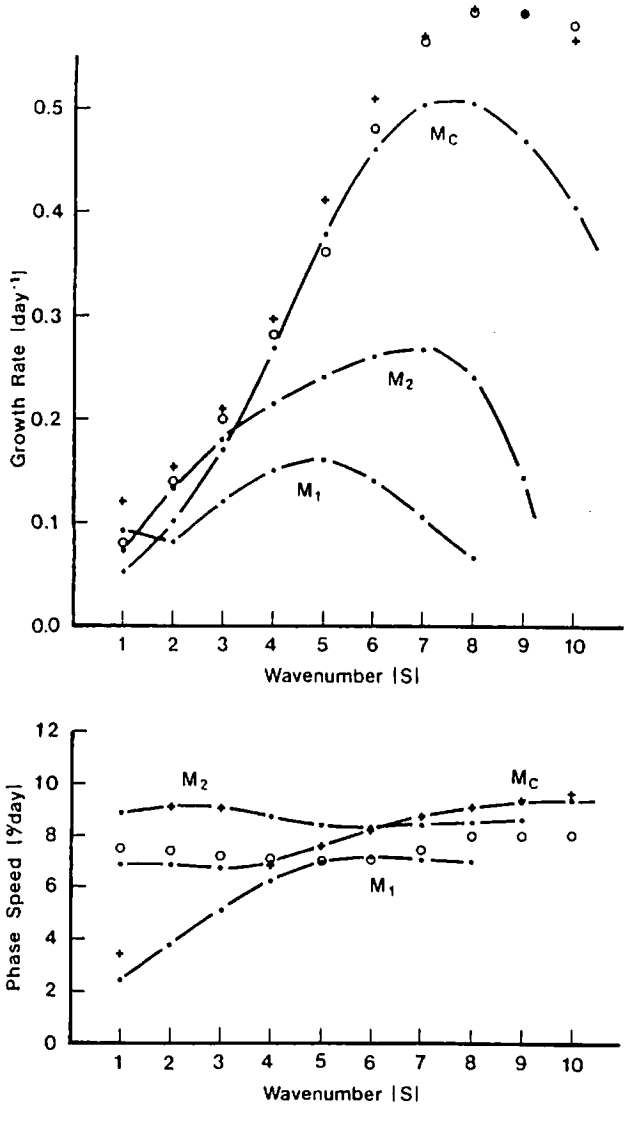


*Fig. 3.* Growth rates and phase speeds of the first-three unstable modes (labeled as $M_C$, $M_2$, and $M_1$) as functions of wavenumbers $s = 1$–$10$ for a zonal basic state of Simmons and Hoskins' 30° jet. The cross marks denote the fastest growing modes for constant static stability profile, $\gamma = 30$ K, and white circles denote the results of Simmons and Hoskins (1976).

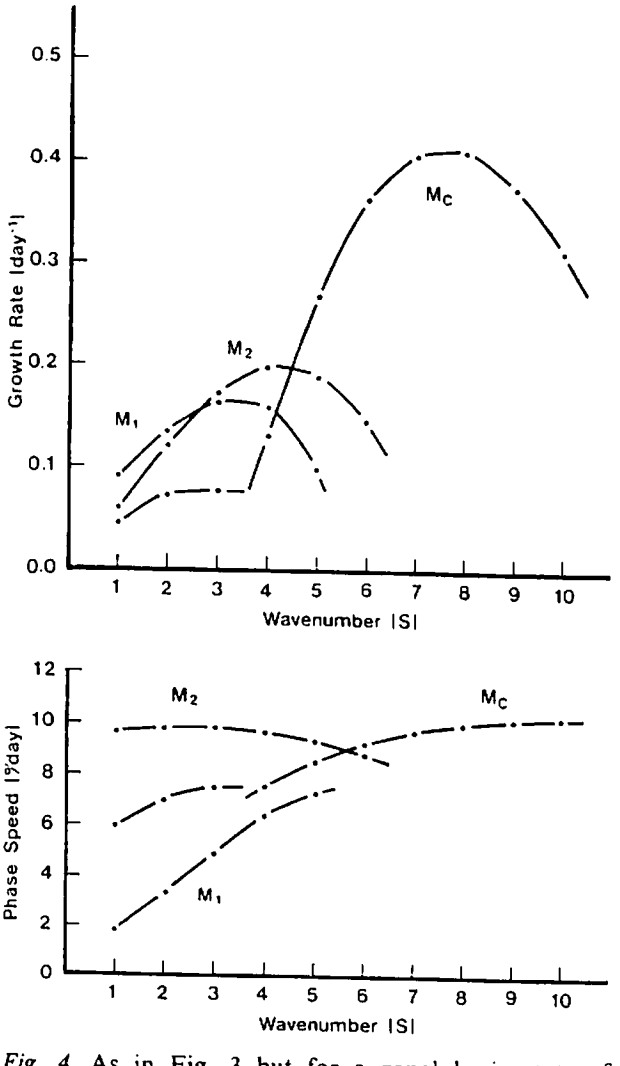


*Fig. 4.* As in Fig. 3 but for a zonal basic state of January 1979. $M_C$ is the shallow Charney mode, and $M_1$, $M_2$ the deep Charney modes.

whereas that of $M_2$ is fast (about 9°/day). The distinct phase speeds of these unstable modes were also detected by Gall (1976) and Zhang and Sasamori (1985).

Fig. 4 illustrates the same curves for the January basic state. For the basic state having a global extension, the unstable modes are partitioned in the northern and southern hemispheric modes by analyzing their structures. The results in Fig. 4 are of the northern hemispheric modes, and a similar result has been obtained by a symmetric extension of the northern basic state toward the Southern Hemisphere. Contrasted with Fig. 3 we find the growth rates of $M_C$ decrease in the planetary waves, and the maximum growth rates of $M_1$ and $M_2$ shift toward the planetary range. As a result, $M_1$ and $M_2$ become the dominant unstable modes at $s = 1$–2 and $s = 3$–4. Further experiments show that the up-scale shifts of $M_1$ and $M_2$ are caused mainly by the small meridional scale of the basic state in the mid- to lower-troposphere resulting from the tropical and polar easterlies. The results are consistent with those documented by Zhang and Sasamori (1985). The shallow Charney mode $M_C$ seems to have changed to the Green mode $M_G$ in the planetary waves (Green, 1960).

### 3.3. Structures

The latitude-height structures of the geopotential field for $M_C$ at $s = 8$ and $M_2$ at $s = 3$ for the 30° jet are illustrated in Fig. 5. As seen in Fig. 3, these are the most unstable modes at these wavenumbers. The structure of wavenumber 8 shows an amplitude maximum near the surface in mid-latitude, indicating a westward phase tilt with height. The tilt implies a northward heat transport, which would release zonal available potential energy. The structure, and thus the eddy heat and momentum transports, is consistent with Simmons and Hoskins' results. We are convinced that the method of 3-D NMF expansion is useful for studying baroclinic instability. At wavenumber 3, the growth rates of $M_2$ and $M_C$ are competitive, and the solution is hardly obtainable with the time integration method as discussed by Simmons and Hoskins. That, however, is not the case for the present eigenvalue problem. The structure of $M_2$ shows a westward phase tilt with height, but indicates a characteristic northwest–southeast phase tilt in the horizontal plane. This phase structure distinguishes $M_2$ from $M_C$. The monopole structure of amplitude becomes dipole in the higher

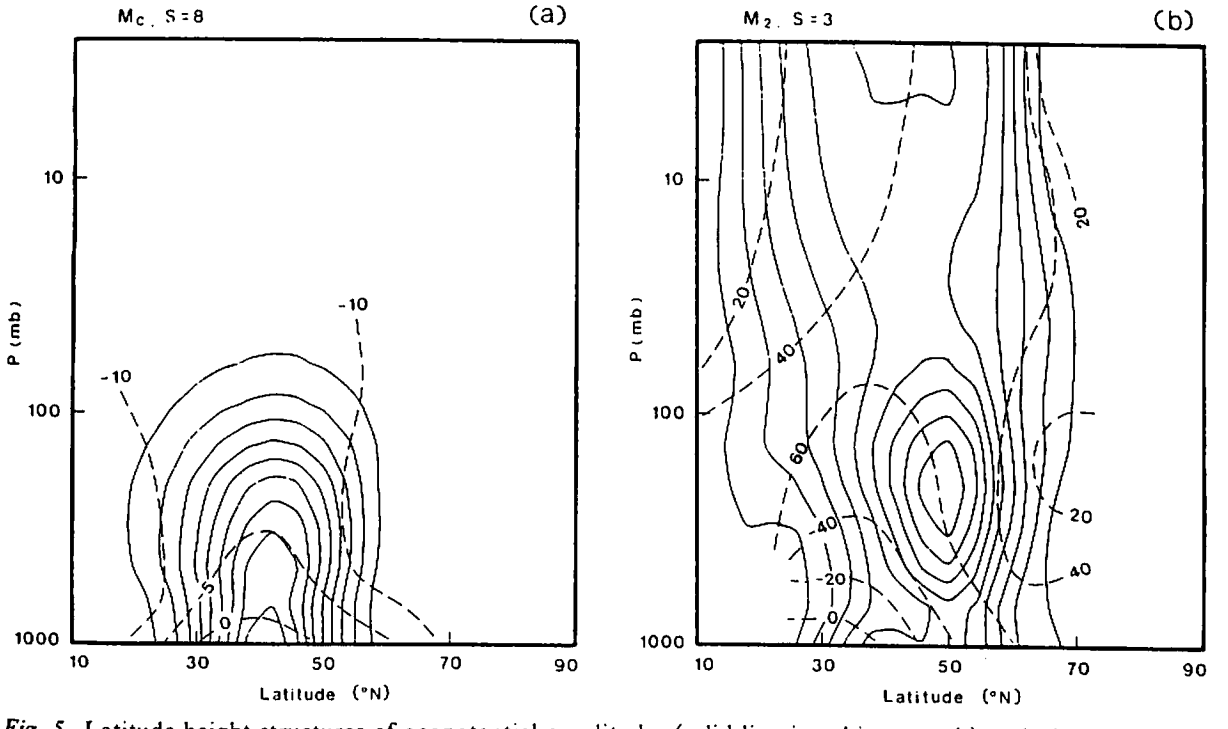


*Fig. 5.* Latitude-height structures of geopotential amplitudes (solid line in arbitrary unit) and phases (dashed line denoting longitudes of ridges) for (a) $M_C$ at wavenumber $s = 8$ and (b) $M_2$ at $s = 3$, with a basic state of Simmons and Hoskins' 30° jet profile.

zonal waves as seen in Simmons and Hoskins' results.

Fig. 6 illustrates the same structures of the fastest growing modes at $s = 6$, 3, and 1 for the January basic state. The structure of $M_C$ at $s = 6$ shows an amplitude maximum at the upper troposphere in mid-latitudes, indicating a westward phase tilt with height. These results resemble those obtained by Hartmann (1979) in which a typical winter basic state is used. The secondary maximum near the upper boundary can be partly due to the truncation in the vertical, although it is not seen in Fig. 5a. For the structure of $M_2$ at $s = 3$, the amplitude maximum shifts northward near 60° N above the tropopause level, indicating a northwest–southeast phase tilt. The phase structure indicates a westward phase tilt with height at mid-latitudes, but the structure is nearly barotropic and out of phase at high latitudes. The structure of $M_1$ at $s = 1$ shows an

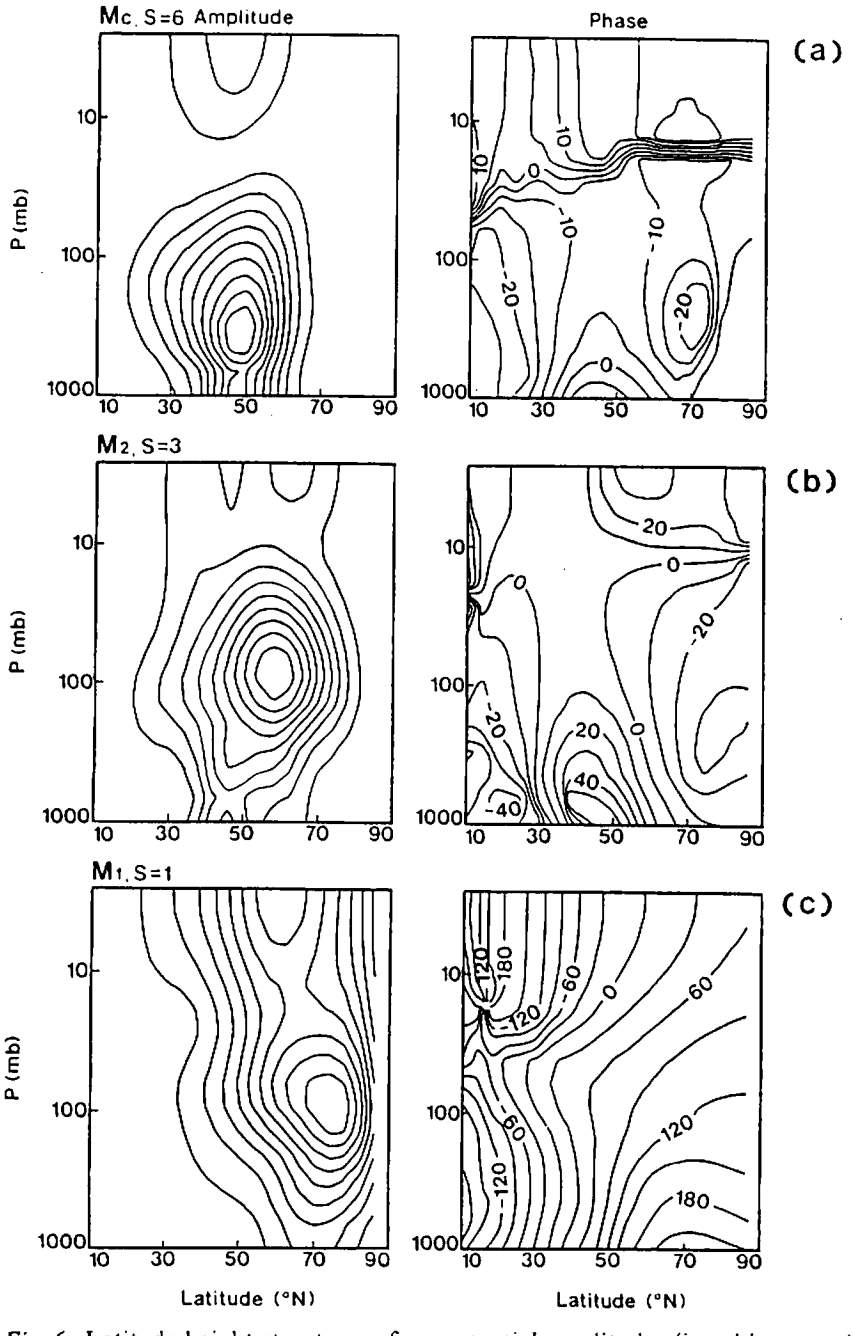


*Fig. 6.* Latitude-height structures of geopotential amplitudes (in arbitrary unit) and phases (longitude of ridge) for (a) $M_C$ at the wavenumber $s = 6$, (b) $M_2$ at $s = 3$, and (c) $M_1$, at $s = 1$ with a zonal basic state of January 1979.

amplitude maximum at 100 mb in high latitudes and another peak in the upper stratosphere, indicating a monotonic westward phase tilt with height. This structure also closely resembles the results obtained by Hartmann (1979) and Zhang and Sasamori (1985), even though the former identifies $M_1$ as the deep Charney mode whereas the latter identifies it as the Green mode. In this study, $M_1$ and $M_2$ are identified as deep Charney modes by the results shown in Figs. 3, 4. In addition, $M_1$ will be characterized by its large external component of $m = 0$, which is typical of external Charney modes, contrasted with the dominant internal component of $m = 1$ for Green mode. The location of high latitudes is necessary for deep Charney modes as Hartmann suggests.

### 3.4. *Energetics*

According to Kasahara and Puri (1981) and Tanaka (1985), an energy $E_i$ for a particular basis function is defined in dimensional form by

$$E_i = \tfrac{1}{2} p_s h_m |w_i|^2. \tag{28}$$

The summation of $E_i$ for all indices $i$ represents a total of kinetic energy and available potential energy integrated over the mass of the atmosphere with an additional boundary term which is, in general, negligible. After a proper normalization of $w_s$, the energy levels for the most unstable modes of $M_1$ at $s = 1$ and $M_C$ at $s = 6$ for the January basic state are plotted as functions of the vertical (Fig. 7a) and meridional (Fig. 7b) indices. The vertical energy spectra reveal bimodal distributions with peaks at $m = 0$ and $m = 2$–4. Energy levels drop significantly at $m = 5$, 6, and contributions from the truncated higher-vertical indices are expected to be small. On the other hand, the largest portion of barotropic energy resides in the meridional indices $l = 3$–6, with some energy gaps in the higher indices. The fact that the energy levels are quite small for both the Kelvin modal indices and the higher indices confirms that the meridional truncation was reasonable. It is interesting to note that these energy spectra of the unstable

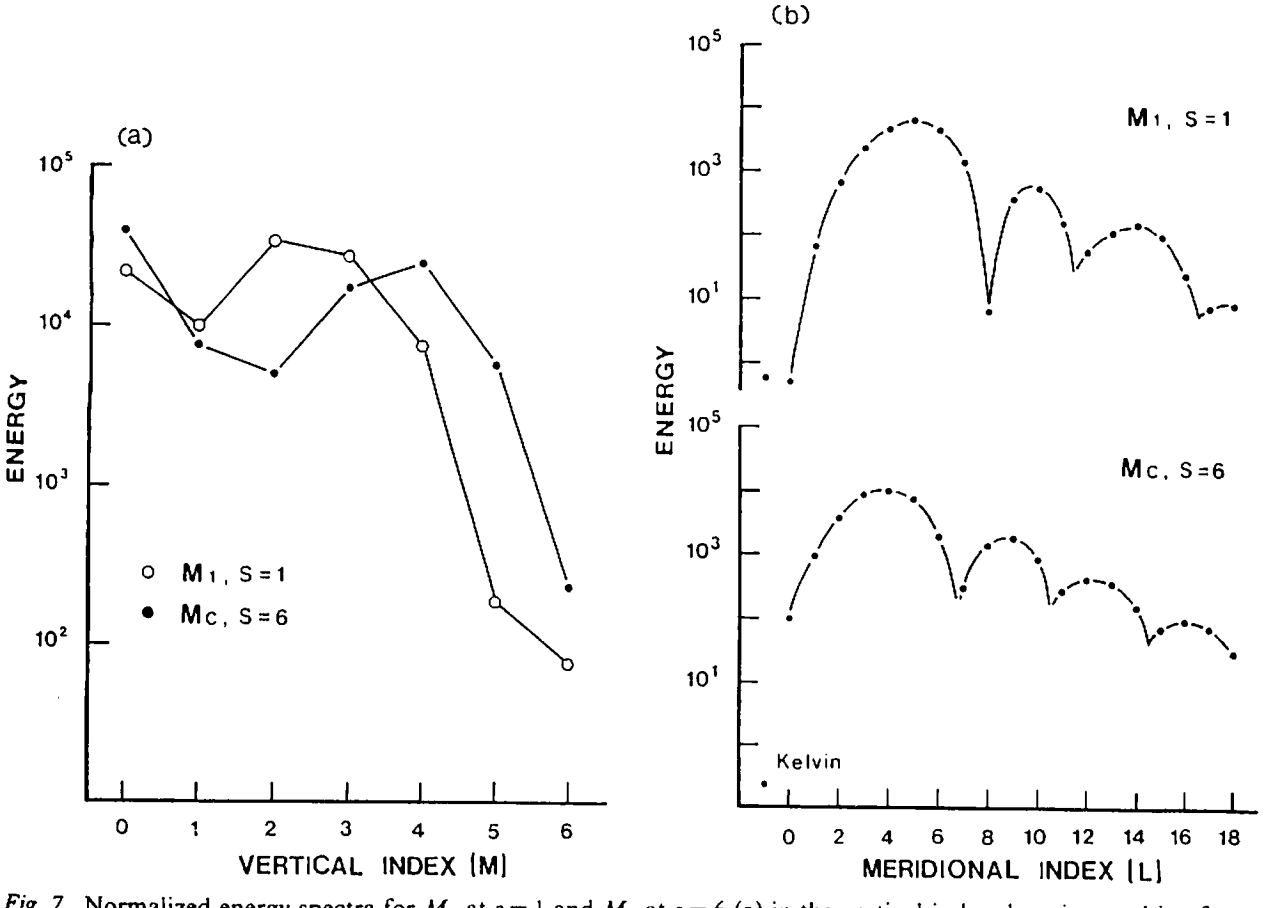


*Fig. 7.* Normalized energy spectra for $M_1$ at $s = 1$ and $M_C$ at $s = 6$ (a) in the vertical index domain, resulting from the summation of all meridional indices, and (b) in the meridional index domain for the barotropic component.

eigensolutions coincide with the spectra observed by Kasahara and Puri (1981) and Tanaka (1985).

Because of the meridional wind shear, not only the baroclinic instability but also the barotropic instability is expected to account for the energy supply of unstable normal modes. In order to explore the origin of this energy supply, an energy flow box diagram describing energy interactions between barotropic and baroclinic components is constructed. By differentiating (28) with respect to time and substituting (22), we obtain

$$\frac{dE_i}{dt} = 2\Omega p_s h_m \sum_j \mathrm{Re}(ib_{ij}^* w_j^* w_i)_{m''=0} + 2\Omega p_s h_m \sum_j \mathrm{Re}(ib_{ij}^* w_j^* w_i)_{m''\neq 0} = C(B_{m''=0}, E_i) + C(B_{m''\neq 0}, E_i). \quad (29)$$

The first term of the right-hand side of (29) stands for energy transformations from the barotropic component of the zonal field $B_{m''=0}$ into $E_i$, and the second term represents those from the baroclinic components of the zonal field $B_{m''\neq 0}$ into $E_i$. By adding all indices $i$ for $m=0$ and for $m\neq 0$, (29) becomes:

$$\frac{dE_{m=0}}{dt} = C(B_{m''=0}, E_{m=0}) + C(B_{m''\neq 0}, E_{m=0}), \quad (30)$$

$$\frac{dE_{m\neq 0}}{dt} = C(B_{m''=0}, E_{m\neq 0}) + C(B_{m''\neq 0}, E_{m\neq 0}). \quad (31)$$

The resulting energy flow box-diagrams are presented in Fig. 8 for the most unstable modes of $M_1$ at $s=1$ and $M_C$ at $s=6$. Upper boxes ($m''\neq 0$, $m\neq 0$) denote the baroclinic components and lower boxes ($m''=0$, $m=0$) the barotropic components. Energy transformations are normalized to yield the percentile contributions to growth. Percentile energy is read in boxes. It is shown that large portions of energy are transformed from zonal baroclinic energy to eddy baroclinic energy for the growing modes. These energy flows essentially result from baroclinic instability, whose major energy source is the available potential energy. The energy supply from $m''\neq 0$ amounts to 84% of the total supply for $M_1$ at $s=1$ and 95% of the supply for $M_C$ at $s=6$. Similar energetics characteristics are obtained for the unstable mode $M_2$ at $s=3$.

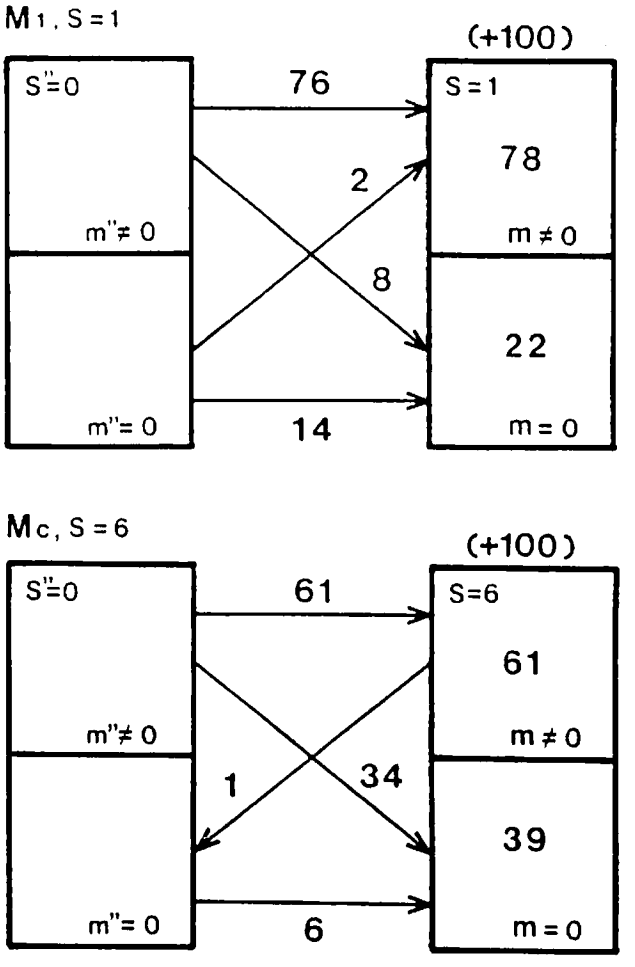


*Fig. 8.* Energy flow box diagrams for $M_1$ at $s=1$ and $M_C$ at $s=6$. Upper boxes ($m''\neq 0$, $m\neq 0$) denote the baroclinic components and lower boxes ($m''=0$, $m=0$) the barotropic components. Left boxes ($s''=0$) are zonal-mean components and the right boxes ($s=1$ and 6) the eddy components. Energy transformations are normalized to yield the percentile contributions of the growth. Percentile energy is read in the boxes.

## 4. Results for a zonally varying basic state

### *4.1. Basic states*

We will consider a zonally varying basic state which is specified by a steady wavenumber 2 superimposed on the zonal-mean basic state. Fig. 9 illustrates the latitude-height section of geopotential height of the wavenumber 2 for January 1979, reproduced by the composition of $m''=0$–6 and $l''=0$–18. We will call this a wave 2 basic state, and distinguish it from the zonal basic state in Fig. 2. It has a global extension, although the figure is illustrated for only the Northern Hemisphere. The amplitude of the wave 2 basic state in the Southern Hemisphere is small. Since

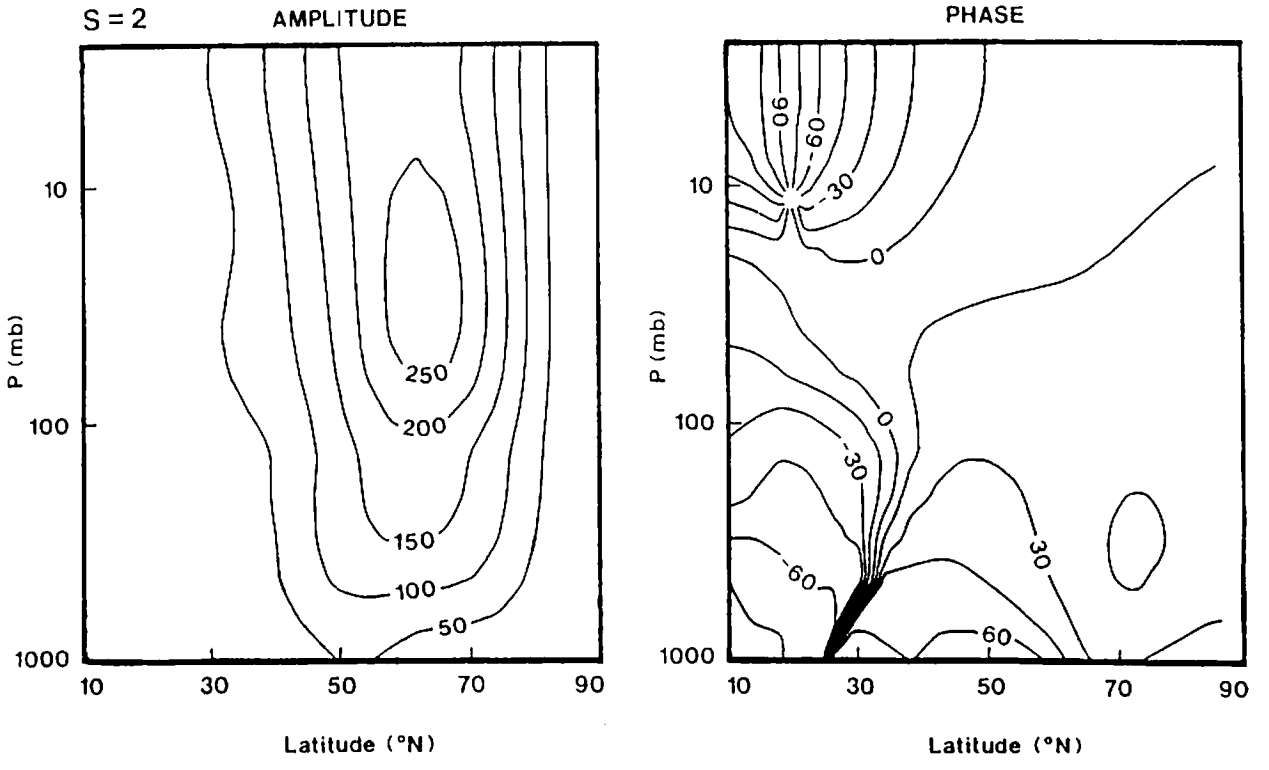


*Fig. 9.* Latitude-height section of geopotential height of the wavenumber 2 for January 1979 used as the basic state. Amplitude ($m$) and phase (longitude of ridge) are reproduced by the composition of $m'' = 0$–$6$ and $l'' = 0$–$18$.

a basic state chosen in this manner involves only even zonal waves ($s'' = 0$ and 2), the eigenspace of (26) becomes a direct sum of eigenspaces for even zonal waves ($s = 0, 2, 4, \ldots$) and odd zonal waves ($s = 1, 3, 5, \ldots$).

### 4.2. *Low-frequency unstable modes*

In this study, we will concentrate on selected low-frequency unstable modes in the planetary waves. The eigenvalue problem (26) is solved first with a zonal truncation of $S = 2$ in order to identify the low-frequency unstable modes. With this truncation, (16) for the odd waves becomes

$$\frac{\mathrm{d}}{\mathrm{d}\tilde{t}} w_1 = -iD_1 w_1 - iB_1 w_1 - iC_1 w_1^*. \qquad (32)$$

Note that (32) is identical to (22) for $s = 1$ except for an additional complex conjugate term arising from the wave 2 basic state. We may thus isolate the effect of the wave 2 basic state on the unstable modes of wavenumber 1. The first term on the right-hand side of (32) indicates phase speeds of neutral modes under a motionless atmosphere. The second term describes zonal-wave interactions. The unstable modes gain their energy through down-scale energy transformations from the zonal field. In contrast, the last complex conjugate term can be recognized as wave–wave interactions, and the growing modes gain their energy through the up-scale energy transformations from the steady zonal asymmetry. Table 3 lists the growth rates and periods of the three fastest-growing modes in the Northern Hemisphere. The results for the zonal basic state are also listed (see Fig. 4). We can identify these low-frequency unstable modes as $M_1$, $M_2$, and $M_G$ of $s = 1$. It is worth noting that the slow-moving mode $M_1$ becomes stationary.

Table 3. *Mode names, growth rates, and eigenperiods of the three fastest-growing modes of $s = 1$ in the zonal basic state (left) and in the nonzonal basic state (right) for the case of zonal truncation $S = 2$*

| Zonal basic state | | | Nonzonal basic state | | |
|---|---|---|---|---|---|
| mode | growth rate (1/day) | period (day) | mode | growth rate (1/day) | period (day) |
| 1 $M_1$ | 0.087 | 181 | 1 $M_1$ | 0.156 | $\infty$ |
| 2 $M_G$ | 0.047 | 61 | 2 $M_G$ | 0.078 | 53 |
| 3 $M_2$ | 0.059 | 37 | 3 $M_2$ | 0.069 | 35 |

Fig. 10 displays the elliptic oscillations of the first-three dominant components of $M_2$ and $M_G$ depicted for the oscillatory factor of $w_{slm}(t)$ in (27). Integers in the parentheses denote $(s, l, m)$, and dots on the trajectories describe the initial phase of the time evolutions. In the zonal basic state these trajectories depict pure circles indicating an eastward propagation. For $M_2$, two barotropic components ($m = 0$) show retrogression with clear principal axes, while the baroclinic component shows progression. The retrogression implies that the Hough mode projection of the eigenmode $M_2$ indicates westward propagation with a period of about 35 days for some dominant barotropic components. The amplitude oscillates in an 18-day period. For $M_G$, the first internal component ($m = 1$) grows significantly during the life-cycle (53-day period), growing 10 times larger than its smallest over a 13-day period. The trajectory is regarded almost as a standing oscillation. The behavior of the first internal component determines the overall structure of $M_G$ as will be shown in the next section.

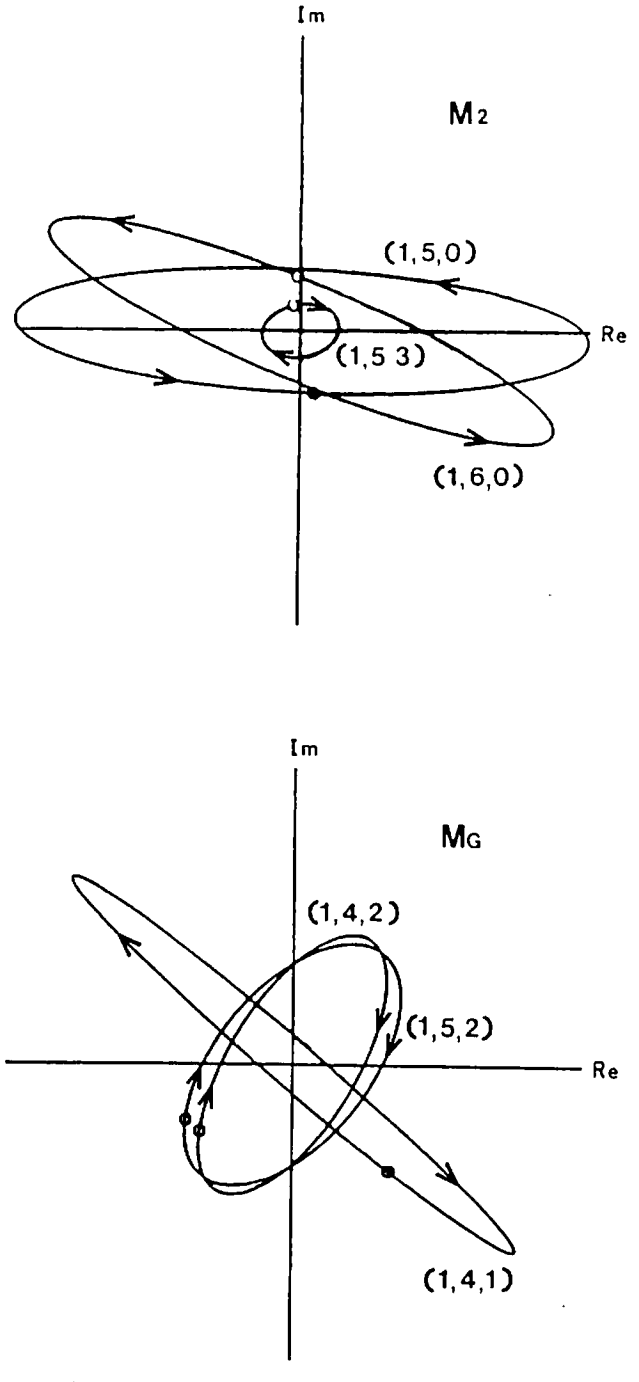


*Fig. 10.* Trajectories of elliptic oscillations of $w_{slm}$ (see eq. 27) on the complex plane for the dominant components of $M_2$ and $M_G$ at $s = 1$. Integers in the parentheses denote $(s, l, m)$, and dots on the orbits indicate the arbitrary initial phases of the time evolution. The expansion coefficients $w_{slm}$ are multiplied by $gh_m$ to have a unit of geopotential.

In order to examine the influence of zonal truncation $S$ on the unstable modes, (26) is now solved with a truncation of $S = 6$. However, we reduced the matrix size by a symmetric extension of the northern basic state toward the Southern Hemisphere, and solved for antisymmetric disturbances. Since the eigenmodes include very fast growing modes of $M_C$ in the synoptic range with relatively high frequency, the following two criteria are imposed in the selection of low-frequency unstable modes: (1) the growth rate must be larger than 0.06 (day$^{-1}$), and (2) the period must be longer than 15 days. Table 4 lists the growth rates and periods of odd wave ($s = 1$, 3, and 5) and even wave ($s = 0$, 2, 4, and 6) solutions which satisfy the above criteria. Results show that the odd waves contain the major low-frequency unstable modes associated with wave-

Table 4. *Mode names, growth rates, and eigenperiods of low-frequency unstable modes of the odd zonal wave solutions (left) and the even zonal wave solutions (right) for the case of the truncation $s = 6$*

| Odd waves | | | Even waves | | |
|---|---|---|---|---|---|
| mode | growth rate (1/day) | period (day) | mode | growth rate (1/day) | period (day) |
| 1 $M_1$ | 0.116 | $\infty$ | 1 | 0.177 | 28 |
| 2 $M_G$ | 0.073 | 56 | 2 | 0.079 | 21 |
| 3 $M_2$ | 0.066 | 39 | 3 | 0.085 | 17 |
| | | | 4 | 0.281 | 16 |

number 1. The stationary mode, the 56-day mode, and the 39-day mode (in period) for the odd wave solutions can be identified as the $M_1$, $M_G$, and $M_2$ modes, respectively.

### 4.3. *Structures*

In conjunction with the component-wise elliptic oscillations in Fig. 10, the total energy of a mode, defined by the summation of $E_i$ in (28), oscillates with a half period of the life-cycle. We may define a mature stage of the modal life-cycle by one of the two energy peaks. Such a definition is not required for the stationary unstable mode except for the alternative sign of the eigenvector. Fig. 11 illustrates the meridional-height structures of the geopotential field for $M_1$, $M_2$, and $M_G$ in the Northern Hemisphere at their mature stages. These are the solutions of $s=1$ in (32)

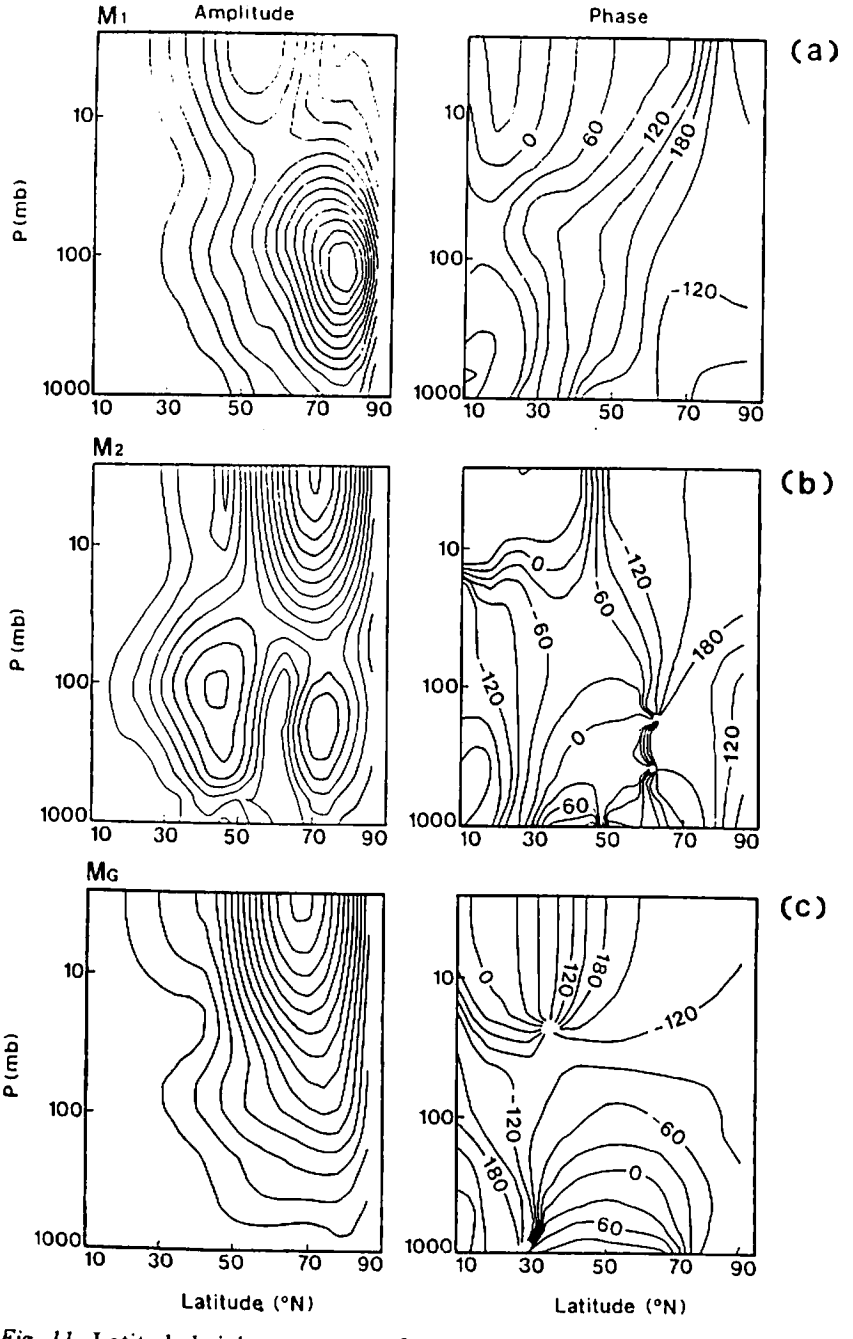


*Fig. 11.* Latitude-height structures of geopotential amplitudes (in arbitrary unit) and phases (longitude of ridges) for (a) $M_1$, (b) $M_2$, and (c) $M_G$ of wavenumber 1 at their mature stages. These are the solutions of (32) which correspond to the zonal truncation $S=2$.

obtained for a global basic state. For the stationary mode $M_1$ the influence of the wave 2 basic state is clear in the phase change, being of equivalent barotropic structure. A pronounced amplitude maximum appears at 75°N, 100 mb level with the ridge around 120°W. Similar stationary modes appear also in Frederiksen (1982) and Simmons et al. (1983). Mode $M_2$ exhibits two amplitude maxima at 75°N and 45°N at the tropopause level with opposite phases. The northern pole produces a ridge around 180°W with a nearly barotropic structure while the southern pole produces a trough around 180°W with baroclinic structure. Moreover, the northern ridge of the solution propagates westward. Contrasted with the monopole structure in the zonal basic state (Fig. 6), we find that the zonal asymmetry of the basic state changes the Charney mode $M_2$ into a dipole structure. Mode $M_G$ produces the amplitude maximum at 65°N in the upper stratosphere with broader meridional extent. The phase tilts westward with altitude. The dominant contribution from $m=1$ of $M_G$ (see Fig. 10) is a typical characteristic of the Green mode even though its nodal structure (Green, 1960) is contaminated by the complicated basic state.

Fig. 12 illustrates the same meridional-height structures of $M_2$ and $M_G$ of $s=1$ but for the truncation of $S=6$. The similarity of the

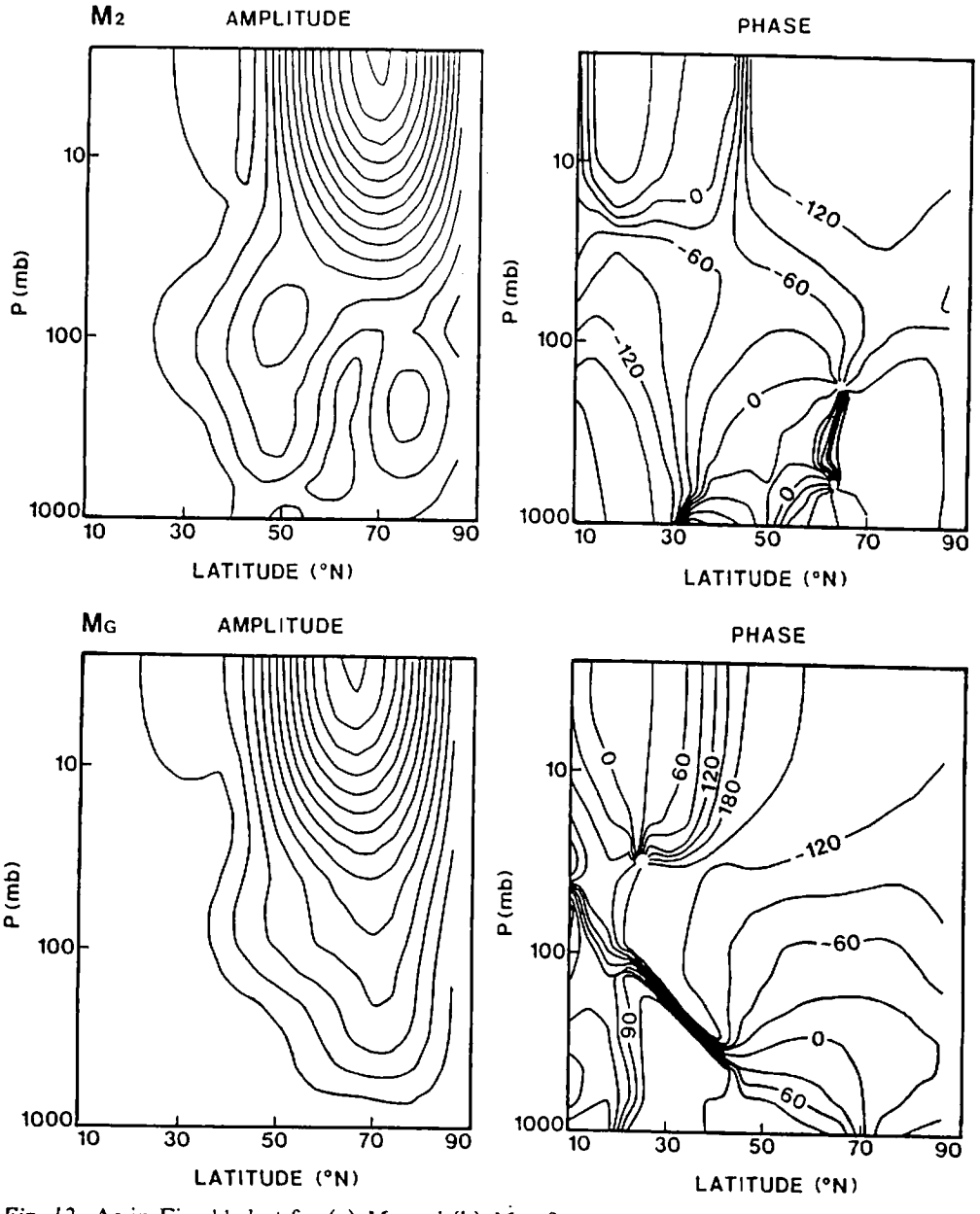


*Fig. 12.* As in Fig. 11, but for (a) $M_2$ and (b) $M_G$ of wavenumber 1 for the case of the zonal truncation $S=6$.

structures shown in Figs. 11 and 12 (refer also to Tables 3, 4) confirms that the solutions are converging with relatively small zonal truncations as far as the low-frequency unstable modes are concerned. The characteristic structure of $M_2$ may be referred to as a dipole Charney mode. Its structure and behavior are similar to the Pacific dipole blockings (e.g., Hansen and Chen, 1982; Kung and Baker, 1986). Also the structure of Green mode $M_G$ is very similar to the occasional amplification event of wavenumber 1 (e.g., Labitzke, 1981; Smith, 1983; Tanaka et al., 1986).

### 4.4. *Energetics*

The energy flow box diagrams of these modes are constructed in much the same way as (30)–(31), including the up-scale energy supply from the wave 2 basic state to wavenumber 1 (Fig. 13). These are the solutions for (32) at the growing stage of their life-cycles. For the stationary mode $M_1$, the barotropic component contains a large amount of energy. The energy transformations from the wave 2 basic state are as large as those from the zonal basic state. For the Green mode $M_G$, the largest portion of energy resides in the baroclinic component. The large energy flow from the zonal baroclinic energy ($s''=0$, $m''\neq 0$) to the eddy baroclinic energy ($s=1$, $m\neq 0$) represents the large transformation of available potential energy from the zonal field to wavenumber 1. The energy and energy flow of the dipole Charney mode $M_2$ are in the middle of $M_1$ and $M_G$. Both the barotropic and baroclinic energy conversions seem to be important for $M_1$ and $M_2$. The present energetics results show that a simple barotropic model is inadequate in describing the essential energy flows of these low-frequency unstable modes.

### 4.5. *Discussion*

Quiroz (1987) provides evidence of the intriguing role of traveling wavenumber 1 in blocking developments. He explains the characteristic westward propagation of the wavenumber 1 by the Rossby–Haurwitz dispersion. The external Rossby waves are basically linear neutral waves, so the energy must be systematically supplied by the interaction process or external forcing. Moreover, the Rossby waves are distorted by a realistic basic state with vertical and meridional shear, where unstable waves may exist as well. In fact, many of the present eigensolutions which are not discussed in this study are the neutral Rossby waves in a realistic basic state. If energy is systematically supplied by the interaction process or external forcing, the unstable planetary waves are more likely to become excited than the neutral Rossby waves in the real atmosphere. The present results suggest that the low-frequency, unstable planetary waves also explain a characteristic structure and westward propagation of wavenumber 1 during the winter.

In this regard, it may be possible to assume that the blockings are caused by exciting low-frequency atmospheric eigenmodes, whose energy source may vary from case to case. The complete physical understanding is, however, ob-

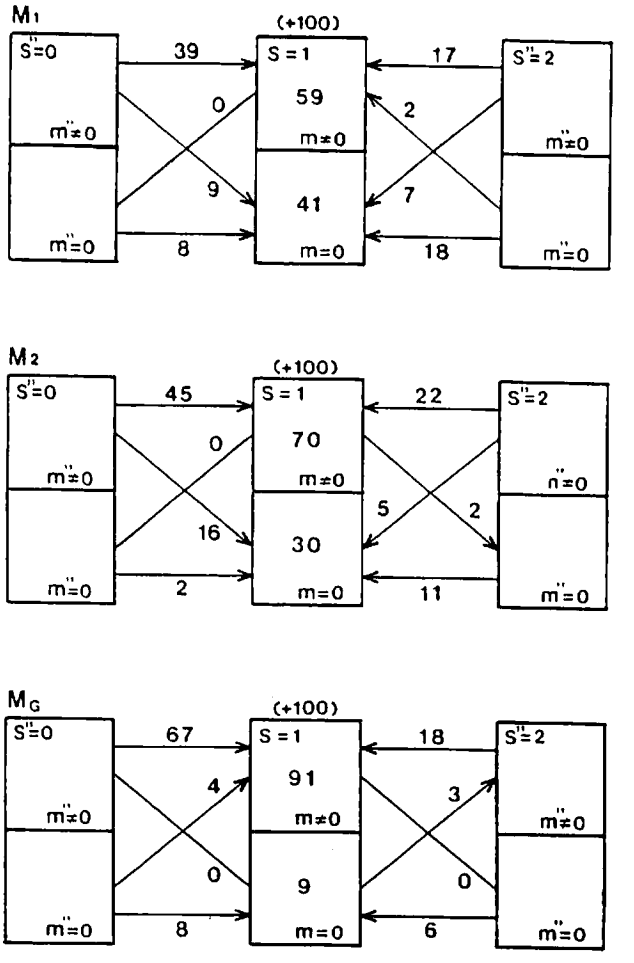


*Fig. 13.* Energy flow box diagrams as in Fig. 8 but for $M_1$, $M_2$, and $M_G$ at $s=1$, including the up-scale energy supply from the wave 2 basic state (right boxes).

scured by the inevitable nonlinearity with complicated energy interactions among a different scale of waves. Recent studies suggest that the importance of the energy supply from transient eddies to low-frequency variabilities, or from synoptic disturbances to planetary waves (e.g., Hansen and Chen, 1982; Shutts, 1983; Kung and Baker, 1986; Holopainen and Fortelius, 1987). Hence, the following speculation may be considered, based on the results of present study combined with our current knowledge: Once the wavenumber 2 is amplified persistently, for instance, by a transition between the multiple equilibrium states (Charney and DeVore, 1979), the high-frequency eddies would organize as the Atlantic and Pacific storm tracks (Frederiksen, 1982), and would provide a systematic, up-scale energy cascade into low-frequency planetary waves (Shutts, 1983). This energy supply might excite the dipole Charney mode $M_2$, which would also have been modulated by the amplified wavenumber 2, to create large-scale blocking at a preferred location. The zonal asymmetry of the time-mean field plays an essential role in this process, and is maintained by the external forcing of surface topography and land–sea thermal contrast. In order to confirm the speculation above, a nonlinear model experiment is in progress, using the three-dimensional spectral primitive equation in terms of the normal mode expansion.

## 5. Concluding summary

This study investigates low-frequency, unstable planetary waves in realistic global states of January 1979, using three-dimensional spectral primitive equations derived by orthonormal vertical structure functions and Hough harmonics. The eigenfrequencies, modal structures, and energetics of the low-frequency, unstable solutions have been contrasted for zonal and zonally varying basic states. Three selected unstable modes are extensively examined. One is the Green mode $M_G$ in the planetary waves, and the other two are the deep Charney modes $M_1$ and $M_2$, which appear to be the second and third fastest growing modes in the synoptic waves with different meridional structures.

There are some discrepancies in the behavior of the planetary-scale unstable modes in the zonal basic state: they propagate eastward, and they are trapped within the troposphere, at least for the most unstable mode (see Hartmann, 1979). Contrasting the results for zonal and zonally varying basic states, we have shown that the zonal asymmetry of the basic state changes the basic features of the low-frequency unstable modes. Their major properties are associated with the properties of wavenumber 1. The Green mode of wavenumber 1 in the zonally varying basic state shows notable transient growth during its life-cycle (56-day) in the first internal vertical component. One of the deep Charney modes $M_1$ turns out to be stationary at a preferred geographical location with nearly barotropic structure. Frederiksen (1982) and Simmons et al. (1983) have analyzed similar stationary modes. The other deep Charney mode $M_2$, which shows a monopole structure in the zonal basic state, becomes a dipole structure during its life-cycle (39-day) in the zonally varying basic state. It is found in this study that the blocking-like dipole modes in Frederiksen and Bell (1987) are identified as a dipole Charney mode modulated by the zonal asymmetry of the basic state. The northern (southern) part of the dipole structure shows westward (eastward) propagation with a periodic growth in amplitude at a preferred location.

The results of the present study suggest that the Rex-type Pacific blockings during the winter are, at least in part, related to the dipole Charney mode modulated by the steady zonal asymmetry of the basic state. It is also noted that the structure and behavior of the Green mode in the stratosphere are similar to the occasional amplification of wavenumber 1 during the winter season, despite the well-known limitation of the linear model. Further study is needed using a comprehensive nonlinear model, as well as the data analysis projecting the atmospheric fields onto these low-frequency unstable modes.

## 6. Acknowledgements

The authors are grateful to V. Peters, G. Vickers, and E. B. Suits for technical assistance. The research was supported by the National Oceanic and Atmospheric Administration under NOAA Grant NA86AA-D-AC114, and the National Science Foundation under NSF Grant ATM-8410487.

## 7. Appendix

*Vertical and meridional resolution tests*

Vertical normal modes for the primitive equations with the basic state at rest are identical to those for the quasi-geostrophic potential vorticity equation on middle-latitude $\beta$-plane. For this reason, the latter equation is used for the vertical resolution test. The linearized equation for meridionally independent perturbations may be written as

$$\frac{f_0^2}{R\gamma}(\sigma^2\phi')' - n^2\phi + \frac{1}{U-C}\left(\beta - \frac{f_0^2}{R\gamma}(\sigma^2 U')'\right)\phi = 0, \qquad \text{(A1)}$$

where $\sigma = p/p_s$, $n = s/a\cos(45°)$, and the primes denote vertical differentiations. Except for the use of $\gamma$ ($= 30$ K) defined in (7), all symbols have their conventional meanings.

The effect of vertical resolutions is then examined for the traditional Charney–Green problem with linear profile of $U$ over $0 < \sigma < 1$ ($U = 30$ m/s at the top). The procedure to solve (A1) is similar to that described in Section 2. Namely, assuming that the atmospheric variables belong to the subspace spanned by the series of vertical structure functions, and taking a natural inner product to obtain a system of ordinary differential equations, we then solve the algebraic matrix eigenvalue problem for the stability analysis. The

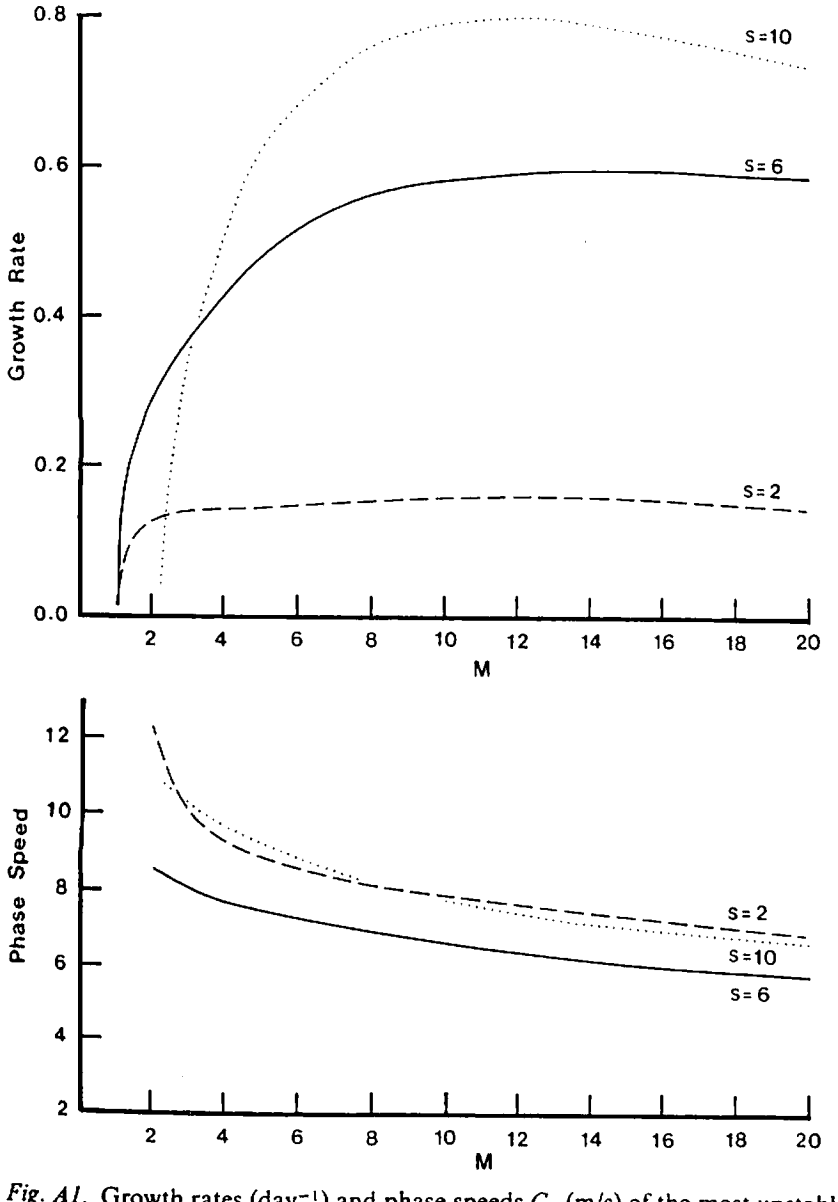


*Fig. A1.* Growth rates (day$^{-1}$) and phase speeds $C_R$ (m/s) of the most unstable modes at wavenumbers $s = 2$, 6, and 10 as functions of vertical resolutions $M$.

results of growth rates and phase speeds for wavenumbers $s = 2$, 6, and 10 are illustrated in Fig. A1 as functions of vertical resolution $M$. As is described in Section 2, we prepare $2M$ vertical structure functions which are computed numerically after Kasahara (1984) using 120 Gaussian vertical levels. Then the first $M+1$ vertical structure functions ($m = 0$–$M$) are used to solve $M+1$ by $M+1$ matrix eigenvalue problems. According to the results, wavenumber 2 seems to have converged with $M = 6$ (at least for the growth rate), although wavenumber 10 requires more vertical resolutions. The results demonstrate that the vertical normal mode expansion is applicable to the instability problem, particularly to the planetary waves.

The effect of meridional truncations and the exclusion of gravity mode basis are examined for the basic state of Simmons and Hoskins' 30° jet using the spectral primitive equations as described in Sections 2 and 3. The vertical advection of perturbation temperature in (5) is neglected here by a scaling analysis. The results of growth rates and phase speeds for the most

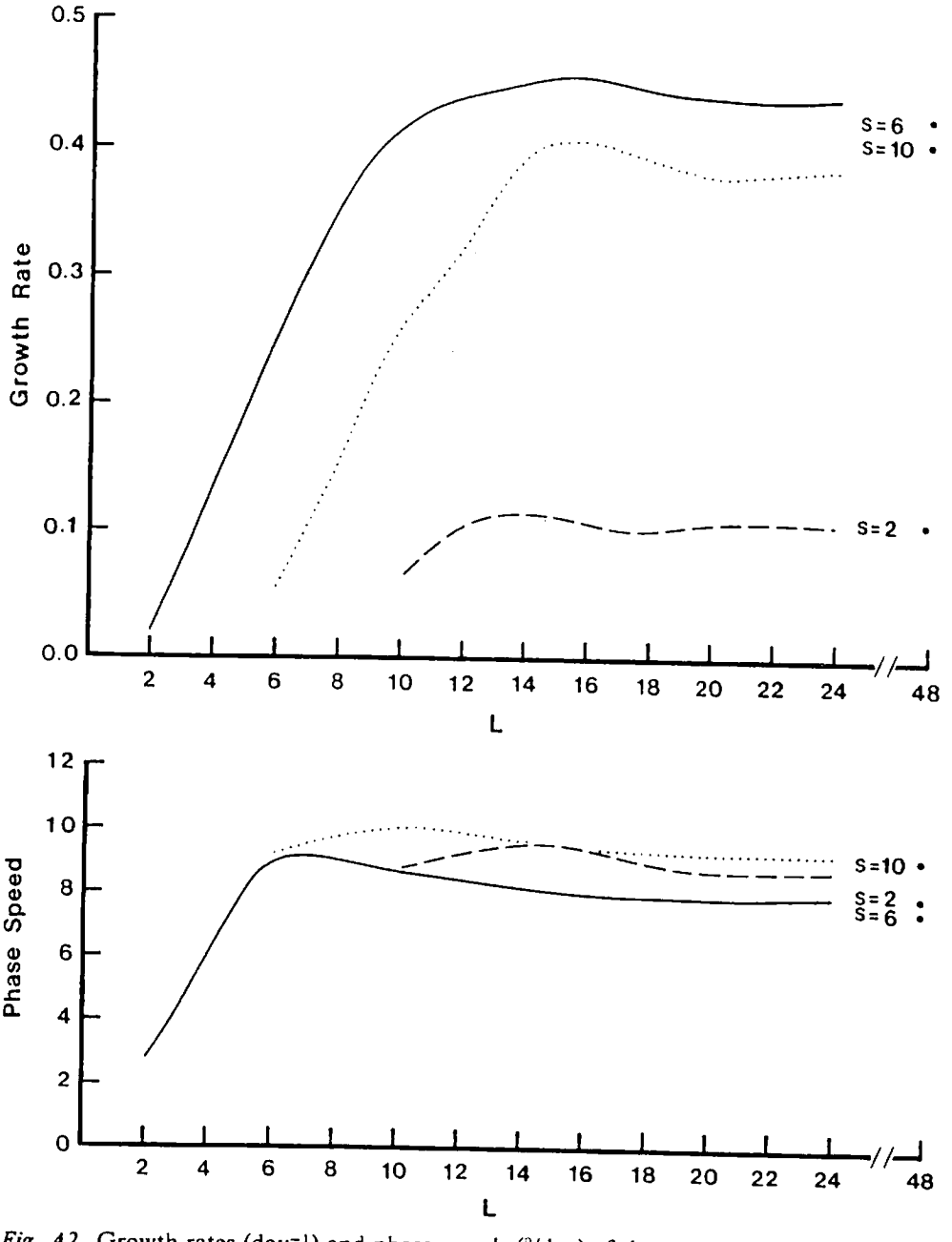


*Fig. A2.* Growth rates (day$^{-1}$) and phase speeds (°/day) of the most unstable modes at wavenumbers $s = 2$, 6, and 10 as functions of meridional truncations $L$. The dots at $L = 48$ represent the results including 24 gravity mode basis added with the Rossby mode basis of $l = 0$–24.

unstable modes at $s = 2$, 6, and 10 are illustrated in Fig. A2 as functions of meridional truncation $L$. The results of $L = 48$ represent the use of Rossby mode basis $l = 0$–24, added with 12 eastward gravity mode basis and 12 westward gravity mode basis. Evidently, the solutions have converged with the truncation $L = 18$, and the gravity mode basis shows insignificant effect on the unstable solutions.

For ageostrophic zonal basic states, such as the January basic state in this study, we obtain high-frequency unstable gravity modes which appear independently of the Charney–Green type instability. Although such unstable gravity modes must be important for the geostrophic adjustment, we have confirmed that the gravity mode basis is unimportant as long as the Charney–Green type instability is concerned.

## REFERENCES


Charney, J. G. 1947. The dynamics of long waves in a baroclinic westerly current. *J. Meteorol. 4*, 135–162.

Charney, J. G. and DeVore, J. G. 1979. Multiple flow equilibria in the atmosphere and blocking. *J. Atmos. Sci. 36*, 1205–1216.

Colucci, S. J. 1985. Explosive cyclogenesis and large-scale circulation change: Implications for atmospheric blocking. *J. Atmos. Sci. 42*, 2701–2717.

Frederiksen, J. S. 1982. A unified three-dimensional instability theory of the onset of blocking and cyclogenesis. *J. Atmos. Sci. 39*, 969–982.

Frederiksen, J. S. and Bell, R. C. 1987. Teleconnection patterns and the roles of baroclinic, barotropic and topographic instability. *J. Atmos. Sci. 44*, 2200–2218.

Gall, R. 1976. A comparison of linear baroclinic instability theory with the eddy statistics of a general circulation model. *J. Atmos. Sci. 33*, 349–373.

Green, J. S. A. 1960. A problem in baroclinic stability. *Quart. J. Roy. Meteorol. Soc. 86*, 237–251.

Hansen, A. R. and Chen, T.-C. 1982. A spectral energetics analysis of atmospheric blocking. *Mon. Wea. Rev. 110*, 1146–1165.

Hartmann, D. L. 1979. Baroclinic instability of realistic zonal-mean states to planetary waves. *J. Atmos. Sci. 36*, 2336–2349.

Holopainen, E. and Fortelius, C. 1987. High-frequency transient eddies and blocking. *J. Atmos. Sci. 44*, 1632–1645.

Holton, J. R. 1975. *The dynamic meteorology of the stratosphere and mesosphere*. Meteorol. Monogr., 37. Amer. Meteorol Soc., 218 pp.

Ioannou, P. and Lindzen, R. S. 1986. Baroclinic instability in the presence of barotropic jets. *J. Atmos. Sci. 43*, 2999–3014.

Kasahara, A. 1984. The linear response of a stratified global atmosphere to tropical thermal forcing. *J. Atmos. Sci. 41*, 2217–2237.

Kasahara, A. and Puri, K. 1981. Spectral representation of three-dimensional global data by expansion in normal mode functions. *Mon. Wea. Rev. 109*, 37–51.

Kung, E. C. and Baker, W. E. 1986. Spectral energetics of the observed and simulated northern hemisphere general circulation during blocking episodes. *J. Atmos. Sci. 43*, 2729–2812.

Labitzke, K. 1981. The amplification of height wave 1 in January 1979: A characteristic precondition for the major warming in February. *Mon. Wea. Rev. 109*, 983–989.

Mullen, S. L. 1987. Transient eddy forcing of blocking flows. *J. Atmos. Sci. 44*, 3–22.

Quiroz, R. S. 1987. Traveling waves and regional transitions in blocking activity in the Northern Hemisphere. *Mon. Wea. Rev. 115*, 919–935.

Sasaki, Y. K. and Chang, L. P. 1985. Numerical solution of the vertical structure equation in the normal mode method. *Mon. Wea. Rev. 113*, 782–793.

Schilling, H.-D. 1986. On atmospheric blocking types and blocking numbers. In *Anomalous Atmospheric Flows and Blocking*, Advances in Geophysics, Vol. 29 (eds. R. Benzi, B. Saltzman and A. C. Wiin-Nielsen). Orlando: Academic Press, 71–99.

Shutts, G. J. 1983. The propagation of eddies in diffluent jet streams: Eddy vorticity forcing of blocking flow fields. *Quart. J. Roy. Meteorol. Soc. 109*, 737–761.

Simmons, A. J. and Hoskins, B. J. 1976. Baroclinic instability on the sphere: Normal modes of the primitive and quasi-geostrophic equations. *J. Atmos. Sci. 33*, 1454–1477.

Simmons, A. J., Wallace, J. M. and Branstator, G. W. 1983. Barotropic wave propagation and instability, and atmospheric teleconnection patterns. *J. Atmos. Sci. 40*, 1363–1392.

Smith, A. K. 1983. Observation of wave–wave interactions in the stratosphere. *J. Atmos. Sci. 40*, 2484–2496.

Staniforth, A., Béland, M. and Côté, J. 1985. An analysis of the vertical structure equation in sigma coordinates. *Atmos.-Ocean 23*, 323–358.

Tanaka, H. 1985. Global energetics analysis by expansion into three-dimensional normal mode functions during FGGE winter. *J. Meteorol. Soc. Japan 63*, 180–200.

Tanaka, H., Kung, E. C. and Baker, W. E. 1986. Energetics analysis of the observed and simulated general circulation using three-dimensional normal mode expansions. *Tellus 38A*, 412–428.

Zhang, K.-S. and Sasamori, T. 1985. A linear stability analysis of the stratospheric and mesospheric zonal mean state in winter and summer. *J. Atmos. Sci. 42*, 2728–2750.